



Review Article

Chemoreception and neuroplasticity in respiratory circuits



William H. Barnett ^a, Ana P. Abdala ^b, Julian F.R. Paton ^b, Ilya A. Rybak ^c, Daniel B. Zoccal ^d, Yaroslav I. Molkov ^{a,*}

^a Georgia State University, Atlanta, GA, United States

^b School of Physiology, Pharmacology and Neuroscience, University of Bristol, UK

^c Drexel University College of Medicine, Philadelphia, PA, United States

^d São Paulo State University, Araraquara, Brazil

ARTICLE INFO

Article history:

Received 30 November 2015
 Received in revised form 22 April 2016
 Accepted 26 May 2016
 Available online 27 May 2016

Keywords:

Respiration
 Obstructive sleep apnea
 Hypertension
 Chronic intermittent hypoxia
 Peripheral chemoreception
 Plasticity

ABSTRACT

The respiratory central pattern generator must respond to chemosensory cues to maintain oxygen (O₂) and carbon dioxide (CO₂) homeostasis in the blood and tissues. To do this, sensorial cells located in the periphery and central nervous system monitor the arterial partial pressure of O₂ and CO₂ and initiate respiratory and autonomic reflex adjustments in conditions of hypoxia and hypercapnia. In conditions of chronic intermittent hypoxia (CIH), repeated peripheral chemoreceptor input mediated by the nucleus of the solitary tract induces plastic changes in respiratory circuits that alter baseline respiratory and sympathetic motor outputs and result in chemoreflex sensitization, active expiration, and arterial hypertension. Herein, we explored the hypothesis that the CIH-induced neuroplasticity primarily consists of increased excitability of pre-inspiratory/inspiratory neurons in the pre-Bötzinger complex. To evaluate this hypothesis and elucidate neural mechanisms for the emergence of active expiration and sympathetic overactivity in CIH-treated animals, we extended a previously developed computational model of the brainstem respiratory-sympathetic network to reproduce experimental data on peripheral and central chemoreflexes post-CIH. The model incorporated neuronal connections between the 2nd-order NTS neurons and peripheral chemoreceptors afferents, the respiratory pattern generator, and sympathetic neurons in the rostral ventrolateral medulla in order to capture key features of sympathetic and respiratory responses to peripheral chemoreflex stimulation. Our model identifies the potential neuronal groups recruited during peripheral chemoreflex stimulation that may be required for the development of inspiratory, expiratory and sympathetic reflex responses. Moreover, our model predicts that pre-inspiratory neurons in the pre-Bötzinger complex experience plasticity of channel expression due to excessive excitation during peripheral chemoreflex. Simulations also show that, due to positive interactions between pre-inspiratory neurons in the pre-Bötzinger complex and expiratory neurons in the retrotrapezoid nucleus, increased excitability of the former may lead to the emergence of the active expiratory pattern at normal CO₂ levels found after CIH exposure. We conclude that neuronal type specific neuroplasticity in the pre-Bötzinger complex induced by repetitive episodes of peripheral chemoreceptor activation by hypoxia may contribute to the development of sympathetic over-activity and hypertension.

© 2016 Elsevier Inc. All rights reserved.

Contents

1.	Introduction	154
2.	Methods	154
2.1.	Experimental data	154
2.1.1.	Animals and ethical approval	154
2.1.2.	Chronic intermittent hypoxia (CIH)	155
2.1.3.	<i>In situ</i> arterially perfused preparation of decerebrate rats	155
2.1.4.	Peripheral chemoreflex activation	155
2.1.5.	Statistical analyses	155
2.2.	Modeling and simulations.	155

* Corresponding author at: Department of Mathematics and Statistics, Georgia State University, 30 Pryor St SW, 750-COE, Atlanta, GA 30303, United States.
 E-mail address: ymolkov@gsu.edu (Y.I. Molkov).

3. Results	156
3.1. Peripheral chemoreflex, respiratory and sympathetic adjustments and exposure to chronic intermittent hypoxia: experimental evidence	156
3.1.1. Effects of CIH on CO ₂ threshold for apnea and active expiration in rats <i>in situ</i>	156
3.1.2. Respiratory and sympathetic adjustments elicited by peripheral chemoreflex activation	157
3.1.3. Exaggerated respiratory and sympathetic chemoreflex responses after CIH exposure	157
3.1.4. Pre-I/I neurons in spontaneously hypertensive rats	158
3.2. Effects of peripheral chemoreceptor activation on the brainstem respiratory and sympathetic networks: insights from computational modeling	158
3.2.1. Model description	158
3.2.2. Simulation of peripheral chemoreceptor activation in naïve rats.	160
3.2.3. Simulation of transient activation of peripheral chemoreceptors in naïve rats with RTN suppressed.	160
3.2.4. Simulation of transient activation of peripheral chemoreceptors in CIH rats	161
3.2.5. Simulation of progressive hypercapnia and hypocapnia in the naïve model and the CIH model.	161
4. Discussion	161
4.1. Peripheral chemoreflex in control rats	162
4.2. CIH-induced central and peripheral plasticity	162
5. Summary and conclusions	163
Acknowledgements	163
References.	163

1. Introduction

Hypertension is a highly prevalent public health problem that affects a large proportion of population worldwide (Kearney et al., 2005; Carey, 2013; Go et al., 2014). Accumulating evidence shows that reducing sympathetic nerve activity decreases blood pressure in hypertensive patients, especially in those who are resistant to pharmacologic antihypertensive treatment (Esler, 2009; Fisher and Paton, 2012), suggesting that sympathetic overactivity is a major contributor to the development and maintenance of hypertension. Moreover, experimental data indicate that increased activity of the sympathetic nervous system is pivotal for the development of high blood pressure in rodent models of hypertension (Simms et al., 2009; Malpas, 2010; Briant et al., 2015). This scenario of hypertension and sympathetic overactivity is observed in obstructive sleep apnea (OSA) patients (Narkiewicz et al., 1998). OSA is a condition characterized by recurrent upper airway collapses during sleep and affects approximately 20% of adult population in USA (Konecny and Somers, 2011). Untreated OSA has cumulative effects on the cardiovascular system, leading to augmented baseline sympathetic activity and arterial hypertension that can be refractory to pharmacological therapies (Williams et al., 2010; Pedrosa et al., 2011). Studies estimate that 50–56% of individuals with OSA are hypertensive (Dudenbostel and Calhoun, 2011).

Clinical and experimental evidence suggests that chronic exposure to intermittent hypoxia (CIH) is a main factor leading to cardiovascular dysfunction in OSA patients (Fletcher, 2001; Caples et al., 2005). In rats, CIH promotes hypertension linked to elevated baseline sympathetic vasomotor tone and higher noradrenaline plasma levels (Braga et al., 2006; Zoccal et al., 2007; Zoccal et al., 2008; Zoccal et al., 2009) highlighting a relationship among CIH, sympathetic overactivity and hypertension. Importantly, the high levels of sympathetic activity of CIH rats were associated with a strengthened coupling between respiratory and sympathetic networks. Indeed, we originally reported (Zoccal et al., 2008) that CIH exposure promotes an increase in sympathetic activity during the expiratory phase, specifically during the late part of expiration (late-E). These additional expiratory bursts in sympathetic activity of CIH rats were coupled to the late-E bursts emerging in the abdominal expiratory motor output. Moreover, the late-E activity was present at rest in eucapnia in CIH-treated animals but never in untreated control animals, and was eliminated by a reduction of CO₂ content in the perfusate (Molkov et al., 2011). The involvement of respiratory-sympathetic interactions in the development of hypertension in CIH rats is further supported by recent findings that late-E modulation in the pre-sympathetic neurons of rostral ventrolateral medulla (RVLM) depends on synaptic inputs from bulbar respiratory neurons rather than on changes in their intrinsic properties (Moraes et al., 2013; Moraes et al., 2014). All

together these data indicate that CIH-induced sympathetic overactivity is linked to the transition of expiration from a passive to an active process at rest. These findings represent novel and unexplored aspects of central mechanisms underpinning arterial hypertension in CIH rats (Moraes et al., 2012b).

The development of arterial hypertension in rats exposed to CIH is fully prevented by previous ablation of carotid body peripheral chemoreceptors (Fletcher et al., 1992), indicating that the plasticity in the neural circuitries of the peripheral chemoreflex, elicited by repeated stimulation during CIH (Moraes et al., 2015), may underpin the development of the observed respiratory and sympathetic changes. Therefore, it is important to understand the neural pathways engaged during peripheral chemoreceptor stimulation in order to identify potential neural mechanisms triggering active expiration and sympathetic overactivity in CIH rats. Here, we discuss the hypothesis that central plasticity accounts for the facilitation of sympathetic and respiratory response to peripheral chemoreflex in CIH conditioned rats. Accordingly, the objectives of this study were (i) to model the neural pathways required for the adjustments in the respiratory and sympathetic motor outputs during peripheral chemoreflex activation, (ii) to understand the functional implications of their repetitive activation during CIH conditioning, and (iii) to shed light on where within the network the neuronal plasticity occurs that is responsible for the sustained active expiration and sympathoactivation following CIH exposure.

2. Methods

In the present study, we combined recent published studies (Braga et al., 2006; Zoccal et al., 2008; Molkov et al., 2011; Moraes et al., 2012a; McBryde et al., 2013; Moraes et al., 2014) and new experimental data obtained in the *in situ* arterially perfused preparation of decerebrate rats, as described in details below.

2.1. Experimental data

2.1.1. Animals and ethical approval

Experiments were performed on male Holtzman rats, weighing 70–90 g, obtained from the Animal Care Unit of the São Paulo State University, Araraquara, and kept at 22 ± 1 °C on a 12-h light/dark cycle (lights on 06:00–lights off 18:00), with access to food and water *ad libitum*. All experimental approaches followed the Guide for the Care and Use of Laboratory Animals published by the US National Institutes of Health (NIH publication No. 85-23 revised 1996) and by the Brazilian National Council for Animal Experimentation Control (CONCEA), and was approved by the Local Ethical Committee in Animal Experimentation (protocol 18/2014).

2.1.2. Chronic intermittent hypoxia (CIH)

The rats were exposed to CIH as previously described (Zoccal et al., 2008). Briefly, the animals were housed in collective cages (maximum of 5 animals per cage) and maintained inside chambers equipped with gas injectors as well as sensors of O₂, CO₂, humidity and temperature, at controlled conditions of temperature (22 ± 1 °C) and humidity (55 ± 10%). The CIH protocol consisted of 5 min of normoxia (FiO₂ of 20.8%) followed by 4 min of pure N₂ injection into the chamber in order to reduce the fraction of inspired O₂ (FiO₂) to 6%, remaining at this level for 40 seconds. After this hypoxic period, pure O₂ was injected to return the FiO₂ back to 20.8%. This 9-minute cycle was repeated 8 h a day (from 9:30 am to 5:30 pm) for 10 days. During the remaining 16 h, the animals were maintained at a FiO₂ of 20.8%. The injections of N₂ and O₂ (White Martins, São Carlos, Brazil) were regulated by a solenoid valve system whose opening-closing control was performed by a computerized system (Oxycycler, Biospherix, USA). In an identical chamber in the same room, the control group was exposed to a FiO₂ of 20.8% 24 h a day for 10 days. The control rats were also exposed to a similar valve noise due to the frequent injection of O₂ to maintain the FiO₂ at 20.8%. In both CIH and control chambers, the gas injections were performed at the upper level of the chamber in order to avoid direct jets of gas impacting on the animals, which could cause stress.

2.1.3. In situ arterially perfused preparation of decerebrate rats

Arterially perfused *in situ* preparations (Paton, 1996) of control and CIH rats were surgically prepared, as previously described (Zoccal et al., 2008). The rats were deeply anesthetized with halothane (AstraZeneca, Cotia, SP, Brazil) until loss of paw withdrawal reflex, transected caudal to the diaphragm, submerged in a chilled Ringer solution (in mM: NaCl, 125; NaHCO₃, 24; KCl, 3; CaCl₂, 2.5; MgSO₄, 1.25; KH₂PO₄, 1.25; dextrose, 10) and decerebrated at the precollicular level. Lungs were removed. Preparations were then transferred to a recording chamber, the descending aorta was cannulated and perfused retrogradely with Ringer solution containing 1.25% Polyethylene glycol (an oncotic agent, Sigma, St Louis, USA) and a neuromuscular blocker (vecuronium bromide, 3–4 µg·ml⁻¹, Cristália Produtos Químicos Farmacêuticos Ltda., São Paulo, Brazil), using a roller pump (Watson-Marlow 502s, Falmouth, Cornwall, UK) via a double-lumen cannula. The perfusion pressure was maintained in the range of 50–70 mm Hg by adjusting the flow rate to 21–25 ml·min⁻¹ and by adding vasopressin to the perfusate (0.6–1.2 nM, Sigma, St. Louis, MO, USA). The perfusate was gassed continuously with 5% CO₂–95% O₂, warmed to 31–32 °C and filtered using a nylon mesh (pore size: 25 µm, Millipore, Billirica, MA, USA). Sympathetic and respiratory nerves were isolated and their activity recorded simultaneously using bipolar glass suction electrodes held in micromanipulators (Narishige, Tokyo, Japan). Left phrenic nerve (PN) discharges were recorded from its central end and its rhythmic ramping activity was used to monitor preparation viability. Left cervical vagus (cVN) and hypoglossal nerves (HN) as well as right thoracic/lumbar abdominal nerves (AbN; T13–L1) were isolated, cut distally and their central activity recorded. Thoracic sympathetic activity was recorded from the left sympathetic chain (tSN) at T8–T12 level. All the signals were amplified, band-pass filtered (0.1–3 kHz; P511, Grass Technologies, Middleton, USA) and acquired in an A/D converter (CED micro 1401, Cambridge Electronic Design, CED, Cambridge, UK) to a computer using Spike 2 software (5 KHz, CED, Cambridge, UK). At the end of the experiments, the perfusion pump was turned off to determine the electrical noise (after the death of the preparations).

All analyses were carried out on rectified and integrated signals (time constant of 50 ms) and performed off-line using Spike 2 software (CED, Cambridge, UK) after noise subtraction. PN burst frequency was determined from the time interval between consecutive integrated phrenic peak bursts and expressed in bursts per minute (bpm). tSN activity was measured as the mean values (in µV) of integrated signals. The changes in the PN burst frequency and tSN in response to peripheral

Table 1

Weights of synaptic connections in the network.

Target population	Excitatory drive [weight of synaptic input] or presynaptic source population [weight of synaptic input from single neuron]
IE(pons)	ramp-I (rVRG) [0.025] ^a
RTN-late-E ^c	Drive CO ₂ [1.08] ^b
RTN-cpg ^c	Drive CO ₂ [1.08] ^b , 2nd Chemo (NTS) [0.1] ^b
RVLM	CVLM [−0.0125] ^a , Drive (VLM) [0.3] ^a , IE (pons) [0.3] ^a , early-I (2) (rVRG) [−0.01], late-E (pFRG) [0.03], 2nd Chemo (NTS) [0.01] ^b , post-I (BotC) [−0.01] ^a , post-I (cVRG) [0.15] ^b
aug-E (BotC)	Drive (pons) [2.7], early-I (1) (pre-BotC) [−0.135], post-I (BotC) [−0.3]
early-I (1) (pre-BotC)	Drive (pons) [1.1] ^a , RTN-cpg [1], aug-E (BotC) [−0.265] ^a , 2nd Chemo (NTS) [0.05] ^b , post-I (BotC) [−0.45], pre-I/I (pre-BotC) [0.1]
early-I (2) (rVRG)	Drive (pons) [2.5], aug-E (BotC) [−0.25], late-E (pFRG)[0.1], post-I (BotC) [−0.5]
late-E (pFRG)	RTN-late-E [0.18] ^b , RTN-cpg [0.12] ^b , early-I (1) (pre-BotC) [−0.0425] ^a , late-E (pFRG) [0.024] ^a , post-I (BotC) [−0.03] ^a , pre-I/I (pre-BotC) [0.015] ^b
2nd Chemo (NTS) ^c	Peripheral Chemoreflex Stimulation [0.75 ^d /1.6 ^e] ^b
post-I (BotC)	Drive (pons) [1.65] ^a , RTN-cpg [0.05] ^b , aug-E (BotC) [−0.01] ^a , early-I (1) (pre-BotC) [−0.025]
post-I (cVRG) ^c	aug-E (BotC) [−0.03] ^b , early-I (1) (pre-BotC) [−0.05] ^b , 2nd Chemo [0.0375] ^b
post-I (e) (BotC)	Drive (pons) [1] ^a , aug-E (BotC) [−0.2] ^a , early-I (2) (rVRG) [−0.01] ^a
pre-I/I (pre-BotC)	Drive (pons) [0.7] ^a , Drive (raphe) [0.3], RTN-cpg [0.11] ^a , aug-E (BotC) [−0.06], late-E (pFRG) [0.018] ^a , 2nd Chemo (NTS) [0.02] ^b , post-I (BotC) [0.16], pre-I/I (pre-BotC) [0.03]
ramp-I (rVRG)	Drive (pons) [2], aug-E (BotC) [−0.1], early-I (2) (rVRG) [−0.3], post-I (BotC) [−2], pre-I/I (pre-BotC) [0.12]

^a Weights that differ in value from Molkov et al. (2011).

^b Projections that did not exist in Molkov et al. (2011).

^c New populations that did not exist in Molkov et al. (2011) or (Molkov et al. (2010).

^d Chemosensory drive for control simulations during peripheral chemoreflex.

^e Chemosensory drive for CIH simulations during peripheral chemoreflex.

chemoreflex activation were expressed as percentage values in relation to basal values prior to the stimulus.

2.1.4. Peripheral chemoreflex activation

Peripheral chemoreceptors were stimulated in the *in situ* preparations by injections of potassium cyanide (KCN 0.05%, 50 µl) into the descending aorta via the perfusion cannula as described previously (Costa-Silva et al., 2010). Stimulation of the peripheral chemoreflex receptors by KCN produced consistent autonomic and respiratory responses, which present low variability within and among the experiments.

2.1.5. Statistical analyses

The data were expressed as mean ± standard error of mean (SEM). Before analysis, data distribution was tested using the Shapiro-Wilk normality test. The sympathoexcitatory and tachypneic responses to peripheral chemoreceptor activation in control and CIH rats were compared using, unpaired Student's *t*-test or two-way ANOVA for repeated measurements followed by Newman-Keuls post-test, respectively. The analysis was carried out using GraphPad Prism software (version 5, La Jolla, CA, USA) and differences were considered significant at *P* < 0.05.

2.2. Modeling and simulations

The model presented here is based on a previous model of central chemoreceptor sensitization from (Molkov et al., 2011; Molkov et al., 2014b), which in turn combined a model describing the origin of abdominal late-E activity (Molkov et al., 2010) and a model describing sympathy-respiratory coupling in the context of the baroreflex (Baekey et al., 2010). All of these models descend from the model described by Rybak et al. (2007) and Smith et al. (2007), which explains the change in respiratory patterns due to successive pontine and medullary transections performed in rats. Most neuronal populations were

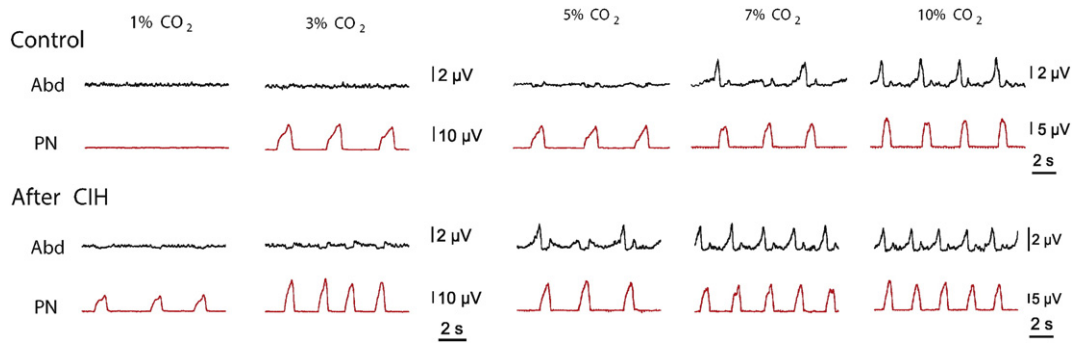


Fig. 1. Recordings depict activity of PN and AbN under progressive hypocapnia and hypercapnia in *in situ* preparations of control and CIH rats. The hypercapnic threshold for emergence of late-expiratory activity in AbN decreases after CIH. The hypocapnic threshold for the appearance of respiratory activity in PN is also decreased in CIH rats. Adapted from [Molkov et al., \(2011\)](#).

composed of single-compartment Hodgkin-Huxley style neuronal models. Each population contained 20 or 50 neurons. Neurons in postsynaptic populations each received input from every neuron in the presynaptic population or the appropriate drive element. The output of certain populations, including motoneurons, was obtained by integrating excitatory synaptic input. Heterogeneity of model parameters and initial conditions (such as membrane potential, calcium concentration, and gating variables) were set by random distributions. Parameters for synaptic weights including changes relative to [Molkov et al. \(2011\)](#) can be found in [Table 1](#).

Simulations were performed using the NSM simulation package version 3.0 developed at Drexel University by S. Markin, I. Rybak, and N. Shevtsova and ported for parallel computing on high-performance clusters using OpenMPI by Y. Molkov. Numerical solutions to ordinary differential equations were computed using the exponential Euler method for integration with a step of 0.1 ms.

3. Results

3.1. Peripheral chemoreflex, respiratory and sympathetic adjustments and exposure to chronic intermittent hypoxia: experimental evidence

3.1.1. Effects of CIH on CO₂ threshold for apnea and active expiration in *in situ*

We previously demonstrated ([Molkov et al., 2011](#)) that rats exposed to chronic intermittent hypoxia exhibit changes in excitability within

the respiratory network. This was verified by the evaluation of the respiratory responses to varying levels of CO₂. [Fig. 1](#) shows the AbN and PN motor patterns in *in situ* preparations of control rats (upper traces) and in rats after CIH conditioning (lower traces) at different CO₂ contents in the perfusate: normocapnia (5% CO₂, middle traces); hypercapnia (7% and 10% CO₂, right traces) and hypocapnia (1% and 3% CO₂, left traces). As it is evident from the figure, in normocapnia control rats exhibited a passive expiratory pattern, as only PN activity showed rhythmic discharges of inspiratory activity, and AbN remained fairly quiescent. With progressive increase in CO₂ large amplitude discharges appeared in the AbN activity of control rats at the late-E phase of the respiratory cycle signifying a transition to active expiration. In CIH-conditioned rats, AbN late-E discharges were present during normocapnia. Lowering CO₂ content to 3% abolished these discharges. So, the CO₂ threshold for transition to active expiration was between 5% and 7% for naïve animals, and between 3% and 5% for the CIH conditioned rats.

As CO₂ level decreased from 3% to 1% the PN rhythmic activity ceased in naïve animals but not in rats exposed to CIH (see first column in [Fig. 1](#), which depicts representative traces from one control rat and one CIH conditioned rat). These results imply that the CO₂ apneic threshold was between 1% and 3% CO₂ in the control group, and below 1% in the CIH animals. Accordingly, both thresholds for apnea and for the transition to active expiration are approximately 2% CO₂ lower in CIH conditioned animals as compared to naïve rats. All data quantification and analyses are presented in details in ([Molkov et al., 2011](#)).

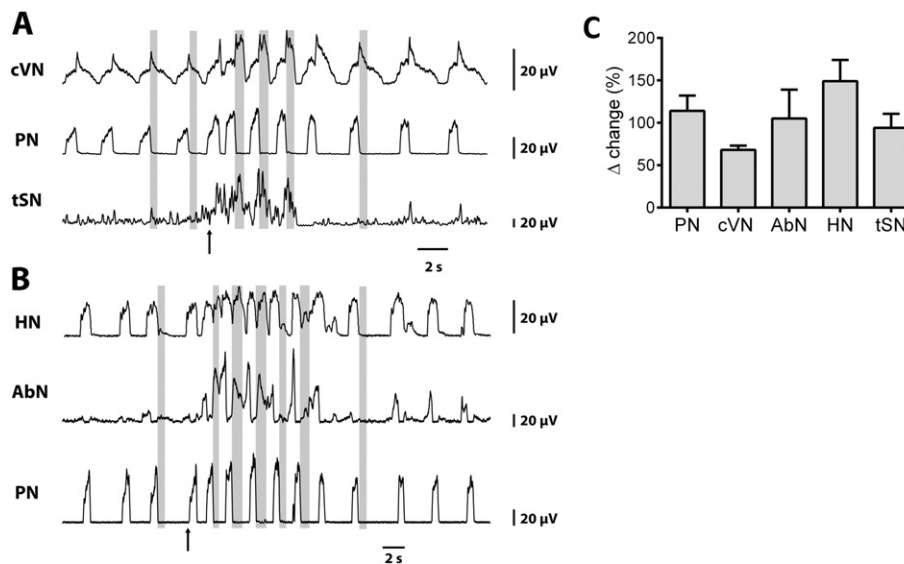


Fig. 2. Appearance of additional motoneuron activation during peripheral chemoreceptor activation. Tracings from two recordings from *in situ* preparations (panels A and B), representative from the group, showing the changes in the HN, cVN, PN, AbN and tSN in response to peripheral chemoreceptor activation by KCN (arrows, 0.05%). Note that during chemoreflex activation, post inspiratory activity increases in cVN and novel post-inspiratory components appears in tSN, AbN, and HN. Late expiratory activity also appears in SN, AbN, and HN. Grey bars highlight post-inspiratory phases of the respiratory cycle. C. Percent changes in amplitude of different motor outputs during peripheral chemoreflex activation.

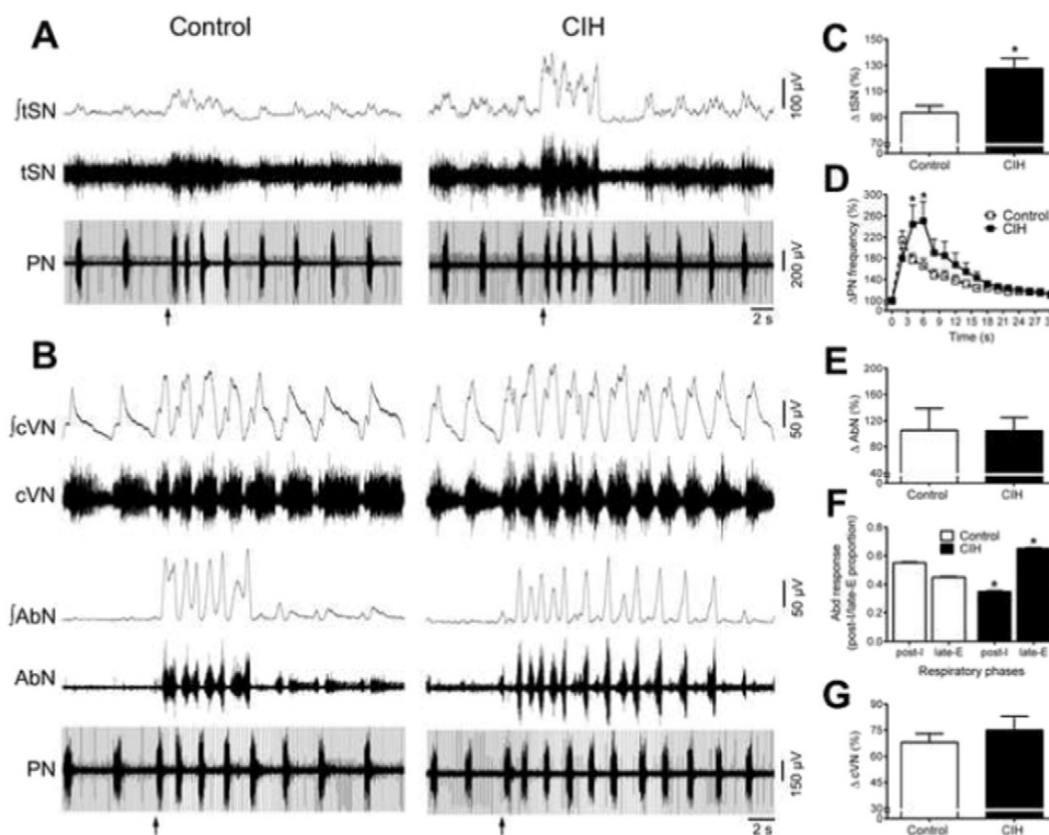


Fig. 3. CIH exaggerates respiratory and sympathetic chemoreflex responses. A. Tracings from control (left) and CIH (right) rats, representative from their respective experimental group, showing the PN and tSN responses to stimulation of the peripheral chemoreflex with KCN (arrows). Note the amplified tSN response during peripheral chemoreceptor stimulation in CIH rats. B. Tracings from control (left) and CIH (right) rats, representative from their respective experimental group, showing the PN and AbN responses to stimulation of the peripheral chemoreflex with KCN (arrows). Note the prolonged AbN response during peripheral chemoreceptor stimulation in CIH rats. C. Percent change in tSN amplitude during peripheral chemoreflex in control and CIH rats. * denotes statistically significant difference. See text for details. D. Time course of the percent change in respiratory frequency relative to baseline after peripheral chemoreceptor activation with KCN for control (open squares) and CIH (filled squares) groups. Data are shown as mean \pm SD. Note prolonged frequency response in CIH group. E. No significant difference in percent change in AbN amplitude during peripheral chemoreflex between control and CIH groups. F. Durations of post-I and late-E expiratory phases relative to the expiration duration in control and CIH groups during peripheral chemoreflex. G. No significant difference in percent change in cVN amplitude during peripheral chemoreflex between control and CIH groups.

3.1.2. Respiratory and sympathetic adjustments elicited by peripheral chemoreflex activation

Previous studies have demonstrated the changes in the pattern of PN, tSN and AbN activities in response peripheral chemoreflex activation (Dick et al., 2004; Moraes et al., 2012a). Herein, we extended this characterization and also evaluated the changes in cVN and HN activities. Transient stimulation of CB peripheral chemoreceptors of control *in situ* preparations with KCN ($n = 7$) had a profound effect on activity patterns in all motor outputs that lasted 10–15s (see Fig. 2 for typical responses). There was an approximately two-fold increase in respiratory frequency (ΔPN frequency: $114 \pm 18\%$, from 22 ± 6 to 46 ± 6 bpm, $P < 0.05$; Fig. 2C) accompanied by augmented amplitude of post-inspiratory discharges recorded from the cVN (ΔcVN : $68 \pm 5\%$, $P < 0.05$, Fig. 2C), and an abrupt rather than decrementing ending as seen during baseline activity. Abdominal, hypoglossal and sympathetic nerve activities also increased mainly during the post-I period (ΔAbN : $105 \pm 34\%$, ΔHN : $149 \pm 25\%$, ΔtSN : $94 \pm 5\%$, $P < 0.05$, Fig. 2C). Importantly, at the end of the stimulus these strong post-I discharges disappeared from all nerves simultaneously suggesting that they may had a common origin. In addition, the AbN and HN exhibited late-E discharges during stimulation that strongly resembles hypercapnia-evoked late-E activity. Similar late-E related discharges were also seen in the sympathetic outflow.

It was previously suggested that the source of late-E AbN activity activated by hypercapnia was in the RTN/pFRG (Janeczowski and Feldman, 2006; Abdala et al., 2009; Molkov et al., 2010). To understand if the AbN

modulation induced by peripheral chemoreflex originates from the same location, Moraes et al. (2012a) suppressed the RTN activity by muscimol (GABA_A receptor agonist) before stimulating peripheral chemoreceptors by KCN. Interestingly, late-E discharges disappeared from both abdominal and sympathetic nerves without affecting the post-I responses. This observation suggests that post-I and late-E activities in AbN and tSN during peripheral chemoreflex have different origins. Late-E activity most probably has the same source as observed during hypercapnia originating from the RTN, whereas the source of post-I activity is located elsewhere.

3.1.3. Exaggerated respiratory and sympathetic chemoreflex responses after CIH exposure

Typical recordings of PN, tSN, AbN and cVN activities of control and CIH rats, illustrating the pattern of changes in response to peripheral chemoreflex activation, are shown in Fig. 3A and B. Consistent with previous observations (Braga et al., 2006), we verified that *in situ* preparations of CIH rats ($n = 8$) exhibited amplified sympathoexcitatory responses to peripheral chemoreflex stimulation (128 ± 8 vs $94 \pm 5\%$, $P < 0.05$, Fig. 3C) in comparison to the control group ($n = 7$). The enhanced sympathetic chemoreflex response in CIH rats also showed augmented respiratory modulation, with bursts occurring preferentially during the post-inspiratory phase. In relation to the PN frequency, the analysis of percentage changes relative to basal values indicated that CIH and control groups presented a similar increase in the magnitude of PN frequency (80 ± 21 vs $114 \pm 18\%$, 2 s after stimulation,

respectively). However, the PN frequency remained elevated at 4 (144 ± 36 vs $77 \pm 12\%$, $P < 0.01$) and 6s (151 ± 36 vs $66 \pm 13\%$, $P < 0.001$) after the stimulation of peripheral chemoreceptors in CIH rats, indicating prolongation of tachypnea (Fig. 3D). With respect to AbN chemoreflex response, the magnitude of increase was similar in both groups (104 ± 21 vs $105 \pm 34\%$, Fig. 3E). However, a different pattern of AbN response is observed in CIH in relation to control rats. In control rats, the relative increase in AbN expiratory activity occurs during the post-inspiration ($55 \pm 2\%$ of the response) and late expiration ($45 \pm 2\%$ of the response), with prevalence in the former ($P < 0.05$, Fig. 3F). In the CIH group, however, the evoked AbN response is shifted towards the late expiratory phase (late expiration: $65 \pm 2\%$ vs post-inspiration: $35 \pm 2\%$, $P < 0.001$, Fig. 3F). The magnitude of increase in cVN in response to KCN was similar between CIH and control groups (75 ± 8 vs $68 \pm 5\%$, respectively, Fig. 3G). Together, these data supports the notion that the processing of sympathetic, inspiratory and late-expiratory responses to peripheral chemoreflex is facilitated in rats exposed to CIH.

3.1.4. Pre-I/I neurons in spontaneously hypertensive rats

In a different animal model of neurogenic hypertension, the spontaneously hypertensive rat (SHR, Moraes et al. (2014) demonstrated that intrinsically bursting neurons in the pre-BötC were found to have altered electrophysiological properties. Specifically, the authors showed that pre-BötC pre-inspiratory neurons are more excitable due to significantly lower conductance of the leak current. Interestingly, SHR and CIH rat models of hypertension share many common features: 1) strengthened respiratory-sympathetic coupling are suggested to be involved in the development/maintenance of arterial hypertension

(Zoccal et al., 2008; Moraes et al., 2014; Briant et al., 2015); 2) the carotid body chemoreceptors play a pivotal role for the development of hypertension (Fletcher et al., 1992; Abdala et al., 2012); 3) the sympathetic response to peripheral chemoreceptors are amplified in SHR and CIH rats (Braga et al., 2006; Simms et al., 2009; Tan et al., 2010; Moraes et al., 2014), suggesting a sensitization of processing of peripheral chemoreceptor inputs; 4) presence of a late-expiratory component in the AbN, in the cervical sympathetic and in the pre-sympathetic RVLM neuronal activity at normal (5%) CO_2 levels strongly resembling the respiratory pattern of control (Wistar) animals at 7% CO_2 (Zoccal et al., 2008; Moraes et al., 2013; Moraes et al., 2014); and 5) a lower apneic threshold compared to Wistar rats (Molkov et al., 2011; Moraes et al., 2014). Based on these similarities, we hypothesize that CIH-conditioned animals have altered baseline respiratory patterns due to increased excitability of pre-I/I population in pre-BötC because of the reduced leak conductance of these neurons (Moraes et al., 2014, 2015). We tested this hypothesis using computational modeling.

3.2. Effects of peripheral chemoreceptor activation on the brainstem respiratory and sympathetic networks: insights from computational modeling

3.2.1. Model description

The main objective of the modeling part of our study was to provide mechanistic interpretation of the processes involved in peripheral chemoreflex modulation of the respiratory and pre-sympathetic networks. This included: (1) an increase in respiratory frequency; (2) the appearance of post-I activity in the HN, AbN, and tSN and an augmentation of post-I activity amplitude in the cVN; (3) the appearance of late-E

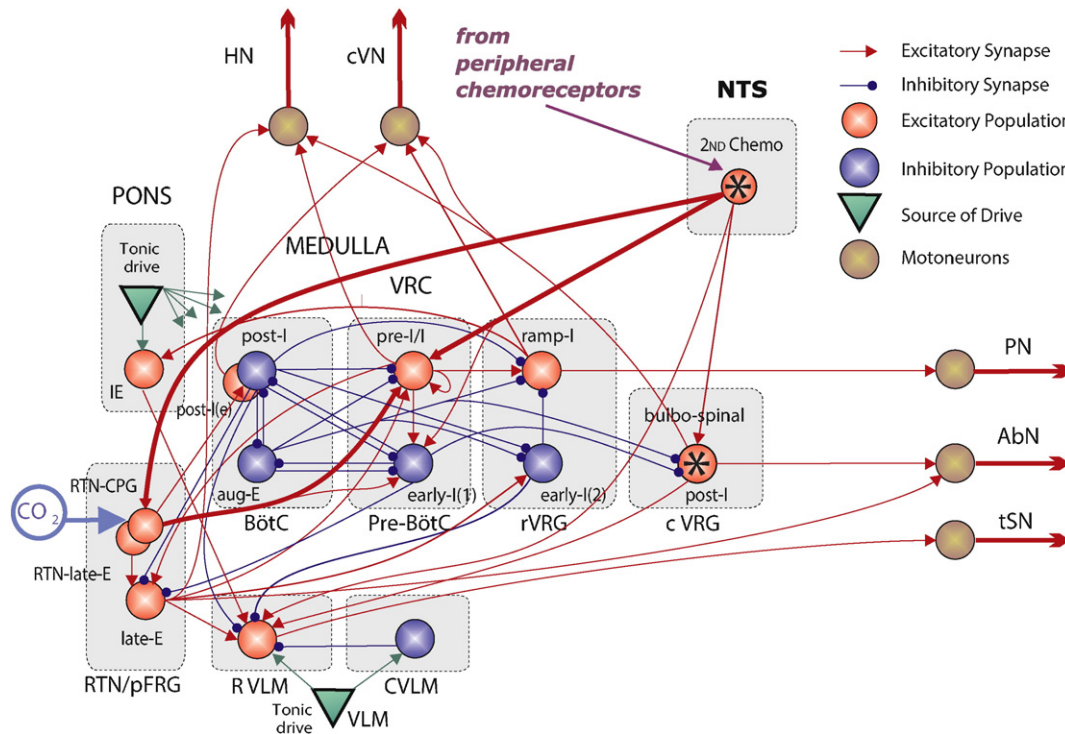


Fig. 4. Network connectivity diagram for model of brainstem respiratory circuits. Brainstem compartments: VRC, ventral respiratory column; BötC, Bötzinger complex; pre-Bötzinger complex; rVRG, rostral ventral respiratory group; cVRG, caudal ventral respiratory group; NTS, nucleus tractus solitarius; RTN/pFRG, retrotrapezoid nucleus/parafacial respiratory group; RVLM, rostral ventrolateral medulla; CVLM, caudal ventrolateral medulla. Neuronal populations: pre-I/I, pre-inspiratory/inspiratory; early-I(1), early inspiratory (1); ramp-I, ramp inspiratory; early-I(2), early inspiratory (2); post-I, post inspiratory; post-I (e), post inspiratory excitatory; aug-E, augmenting expiratory; 2nd Chemo, 2nd-order chemoreceptors; bulbo-spinal post-I, bulbo-spinal post inspiratory; late-E, late expiratory; IE, inspiratory-expiratory phase-spanning; RTN-CPG, CO_2 -sensitive population projecting to CPG and late-E (pFRG); RTN-late-E, CO_2 -sensitive population projecting just to late-E (pFRG). Motoneurons: PN, phrenic nerve; AbN, abdominal nerve; tSN, thoracic sympathetic nerve; HN, hypoglossal nerve; cVN, cervical vagus nerve. Excitatory neural populations, inhibitory neural populations, and excitatory drives are respectively represented as orange spheres, blue spheres, and green triangles. Motoneurons are depicted as brown spheres. Red projections originating in neural populations depict excitatory projections. Blue projections originating in neural populations depict inhibitory projections. Green projections indicate the distribution of excitatory tonic drive. The bold excitatory pathways emphasize converging peripheral chemosensitive projections to the pre-I/I population. Populations that were not included in a previous model are marked with an asterisk.

activity in the HN, AbN, and tSN; and (4) an increase in respiratory-independent activity of tSN.

The model was developed as an extension of previous models (Baekey et al., 2010; Molkov et al., 2011; Rybak et al., 2012; Molkov et al., 2014b) to accommodate a population of 2nd-order cells in the NTS receiving peripheral chemoreceptor inputs and their efferent projection to ventromedullary compartments. The schematic of the extended model is shown in Fig. 4. During peripheral chemoreflex, input from the carotid body (CB) was represented by a constant drive to the 2nd-order NTS neurons. The population of these neurons distributed excitatory projections to the respiratory and sympathetic circuits. To account for the increase in respiratory frequency, which should primarily occur through shortening of the E2 phase, we implemented direct excitation from the 2nd-order NTS neurons to the early-I (1) and pre-I/I populations of the pre-BötC. The pre-I/I population was the primary excitatory population contributing to the initiation of inspiration.

To account for the post-I activity in motoneuron output, we introduced another post-I population (bulbo-spinal cVRG). This population receives tonic excitation from the 2nd-order NTS neurons during peripheral chemoreflex. In addition, the activity of this population was modulated by the respiratory CPG; inhibition from aug-E and early-I (2) shaped its output to allow only post-inspiratory activity. This population received tonic excitation from 2nd-order chemoreceptive neurons in the NTS. Activation of this population during inspiration was prevented by inhibition from early-I (2); activation of this population during E2 was suppressed by inhibition from aug-E. Thus, activation of and excitation from the 2nd-order chemoreceptive NTS neurons translate to post-I activity in the cVRG. This post-I (cVRG) population was responsible for post-I activity in the HN, AbN, and tSN and augments the post-I component in the cVN.

In our previous model, we described how CO₂-sensitive drive from the RTN mediated the central chemoreflex in respiratory circuits (Molkov et al., 2010; Molkov et al., 2011). Increased drive from the RTN could drive the pFRG late-E population to threshold, and in this way, the central chemoreflex induced the onset of bursting activity in the pFRG, which was observed as late-E activity in the AbN. In the extended model, a CO₂-sensitive drive excited two distinct neuronal populations in the RTN (RTN-late-E and RTN-cpg) (see Fig. 4). One of these populations—the RTN-cpg—also received input from 2nd-order NTS chemoreceptive neurons. The dynamics of individual neurons in these two RTN populations were not modeled; rather, we directly simulated the firing rate of the population. The RTN-cpg population projected to: pre-I/I (pre-BötC), early-I (1) (pre-BötC), post-I (BötC), and late-E (pFRG). The RTN-late-E population projected only to the late-E population of the pFRG. Therefore, the pFRG late-E population received excitatory projections from both peripheral chemoreflex sensitive and peripheral chemoreflex insensitive central chemoreceptive populations in the RTN. The CO₂-dependence of RTN-cpg and RTN-late-E were the same and mediated the central chemoreflex in a similar fashion to the direct CO₂-sensitive drive in Molkov et al. (2011). Progressive hypercapnia and hypocapnia were modeled by changing the magnitude of the CO₂ sensitive drive to RTN-cpg and RTN-late-E.

Since stimulation of the peripheral chemoreceptors can initiate late-E activity in the AbN, which is RTN-dependent (Moraes et al., 2012a), we extended the model to include excitation from 2nd-order NTS peripheral chemoreceptive neurons to augment excitatory drive from the RTN to the CPG. We implemented direct projections from the 2nd-order NTS chemoreceptive neurons to the RTN-cpg population. The RTN-cpg population distributed both central and peripheral chemosensory drive to the respiratory circuits. Notice that the RTN-late-E population did not receive excitation from the 2nd-order NTS chemoreceptive neurons, so this component of excitatory input to the pFRG late-E population was dependent on the central chemoreflex but independent of the peripheral chemoreflex.

The model by Baekey et al. (2010) described the baroreflex circuits, including 2nd-order baroreceptive NTS neurons and the pre-

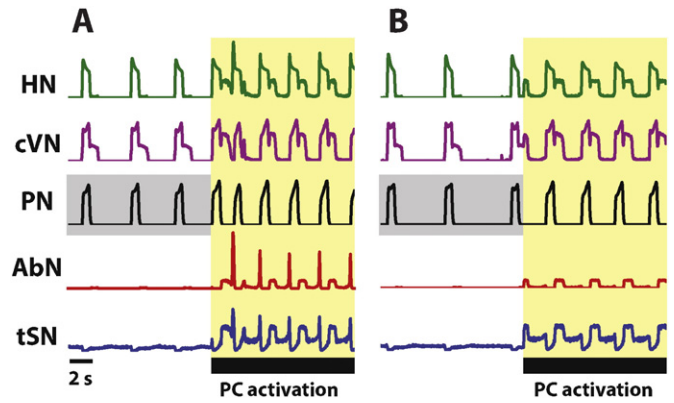


Fig. 5. Simulation depicting the response of motoneuron output (HN, cVN, PN, AbN, and tSN) to the activation of the peripheral chemoreflex (A) and the motoneuron response during suppression of RTN (B). (A) During activation of peripheral chemoreflex, network frequency increases; post-inspiratory activity appears in HN, AbN, and tSN motor nerves, and post-inspiratory activity in cVN increases in amplitude. Late expiratory activity appears in HN, AbN, and tSN. (B) The suppression of the RTN abolishes late-expiratory activity in HN, AbN, and tSN but has little effect on post-I activity. The interval highlighted in yellow corresponds to the duration over which the peripheral chemoreflex is stimulated. Baseline activity of PN is highlighted in grey to emphasize the difference in frequency in the control model and the model with RTN suppressed before the peripheral chemoreflex stimulation.

sympathetic circuits in the ventrolateral medulla. In that model, 2nd-order baroreceptive NTS neurons directly excited the CVLM, which inhibited RVLM to provide sympathoinhibition. Here, we implement a parallel pathway where 2nd-order peripheral chemoreceptive NTS neurons projected directly to the RVLM in order to mediate sympathoexcitation during peripheral chemoreflex for which there was experimental evidence (Aicher et al., 1996; Koshiya and Guyenet, 1996).

As mentioned above, hypercapnia induces late-E activity in the AbN. CIH rats experience a hypocapnic shift in the threshold for emergence of this late-E activity (Abdala et al., 2009; Molkov et al., 2010; Molkov et al., 2011) (Fig. 1). On the other hand, experimental evidence in SHR suggests that the pre-I/I population in the pre-BötC becomes more excitable via a decrease in leak conductance (Moraes et al., 2014). We used this evidence to formulate the hypothesis that repetitive activation of

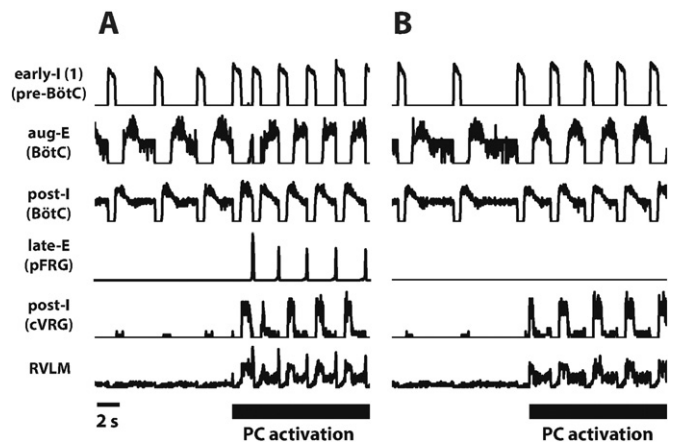


Fig. 6. Simulation of activity of respiratory and sympathetic populations (early-I (1) (pre-BötC), post-I (BötC), aug-E (BötC), late-E (pFRG), and post-I (cVRG)) before and during stimulation of peripheral chemoreflex (A) and the activity of respiratory and sympathetic populations under suppression of RTN during stimulation of peripheral chemoreflex (B). (A) Peripheral chemoreflex increases drive to the respiratory central pattern generator—increases network frequency and activating the late-E (pFRG) and post-I (cVRG) populations. (B) The suppression of RTN for the duration of the simulation abolishes expiratory activity in the late-E (pFRG) population.

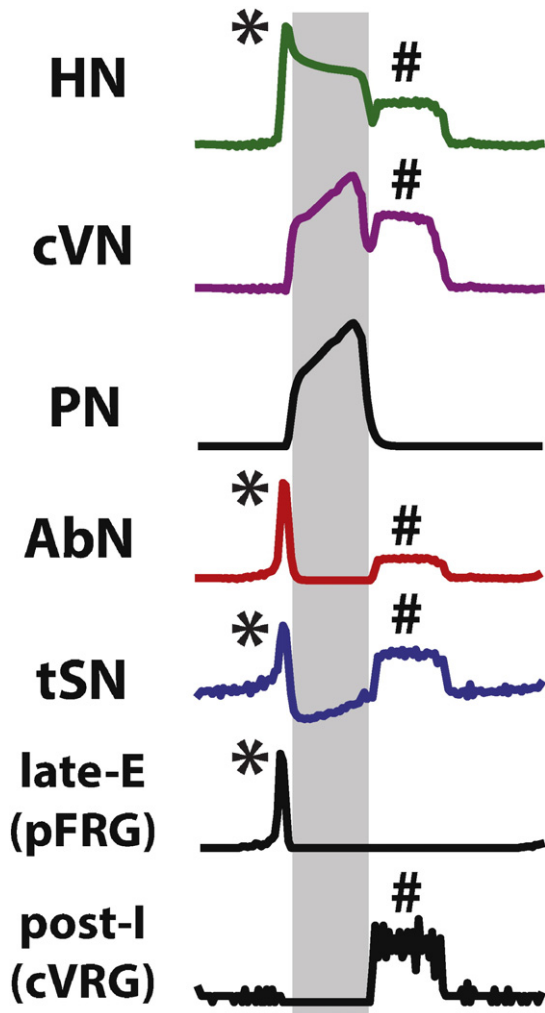


Fig. 7. Blow-up of activity during peripheral chemoreflex in the control model. Motoneuron output is compared to the activity of late-E (pFRG) and post-I (cVRG). Activity during late-E and post-I phases are highlighted in yellow and grey, respectively.

peripheral and, hence, central chemoreceptors during CIH conditioning (due to direct excitatory projections from 2nd order NTS neurons to the RTN central chemoreceptors, see emphasized arrows in Fig. 4) induces plasticity in this population as recently proposed (Moraes et al., 2015; Zoccal, 2015); specifically, we modelled the respiratory plasticity evoked by CIH as a decrease in the leak conductance of the pre-I/I population. The average leak conductance of these neurons was decreased from 2.9 nS in the control model to 2.3 nS in the CIH model. In order for the increase in excitability of the pre-I/I population to contribute to the excitability of the late-E (pFRG) population, we implemented a direct excitatory projection from pre-I/I (pre-BötC) to late-E (pFRG). The relative increase of the sympathoexcitatory response to peripheral chemoreceptor activation was implemented by a change in the chemosensory drive to 2nd-order peripheral chemoreceptive NTS neurons (see Table 1).

3.2.2. Simulation of peripheral chemoreceptor activation in naïve rats

The extended model was used to investigate the effects of peripheral chemoreceptors activation on the respiratory-sympathetic networks. Fig. 5A and Fig. 6A depict the activity of the respiratory circuits during normal conditions and during activation of peripheral chemoreceptors. A square pulse of excitatory drive to the 2nd-order NTS chemoreceptive neurons elicited an increase in network frequency, which was based on

additional excitation to pre-I/I and early-I (1) neurons that overcame inhibition from the inhibitory populations in the BötC and initiated inspiration. Hence, the expiratory phase decreased in duration. Specifically, the duration of bursts in the aug-E and post-I populations of the BötC decreased (Figs. 2, 6A). However, the duration of inspiration (Fig. 5A) and the burst duration of early-I (1) (Fig. 6A) did not change substantially. After peripheral chemoreceptor stimulation, the model captured the appearance of post-I activity in the HN, AbN, and tSN and increased post-I activity in the cVN that are prevalent in experimental recordings (Fig. 7). In the model, this activity was driven by the post-I (cVRG) population; it was silent without input from 2nd-order NTS chemoreceptive neurons, and received respiratory modulation in the form of inhibition from BötC aug-E and strong inhibition from pre-BötC early-I (1) (see Fig. 4). This inhibition occurred in the I-phase and E2-phase of respiration (Fig. 6A).

We propose that 2nd-order NTS chemoreceptive neurons project directly to central chemosensory populations of the RTN. Accordingly, during peripheral chemoreceptor activation, the CO₂ sensitive drive from RTN-cpg to the respiratory circuits was augmented. Hence, the pathway for stimulation of the late-E (pFRG) population became active (Fig. 6A). The model captured the appearance of late-E activity in the HN, AbN, and tSN that is prevalent in experimental recordings. The increase in drive to the pFRG was sufficient to induce periodic bursts of activity immediately preceding each inspiratory burst (Fig. 7). Tonic and respiratory-modulated activity in tSN during peripheral chemoreceptor activation increased due to converging direct and indirect excitatory pathways to RVLM. RVLM possessed a strong post-I component due to excitation from the post-I population in cVRG and a late-E component originating from the pFRG (Fig. 7).

3.2.3. Simulation of transient activation of peripheral chemoreceptors in naïve rats with RTN suppressed

Evidence suggests that late-E activity in the AbN during hypercapnia is dependent on an excitatory drive from the RTN (Molkov et al., 2010; Moraes et al., 2012a). Moreover, late-E activity in the AbN is abolished upon suppression of the RTN (Moraes et al., 2012a). Here, we reproduce experimental results of RTN suppression in the model. Fig. 5B and Fig. 6B depict activation of peripheral chemoreceptors with the RTN suppressed. To simulate the effects of muscimol injected in the RTN, we inhibited the central chemosensory populations in the RTN and the late-E population in pFRG. This manipulation was mimicked by reducing the CO₂ sensitive drive to RTN-cpg and RTN-late-E by 20%. Input from 2nd-order NTS peripheral chemoreceptive neurons to the central chemosensory complex in the RTN was not able to overcome inhibition by muscimol and activate the late-E population. The activation of the post-I population in the cVRG and the projections from the 2nd-order NTS chemoreceptive neurons into the respiratory CPG and pre-sympathetic groups was unaffected by suppression of the RTN (Fig. 5B and Fig. 6B). Due to the inhibition of the RTN, the late-E population in the pFRG remained silent during peripheral chemoreceptor activation

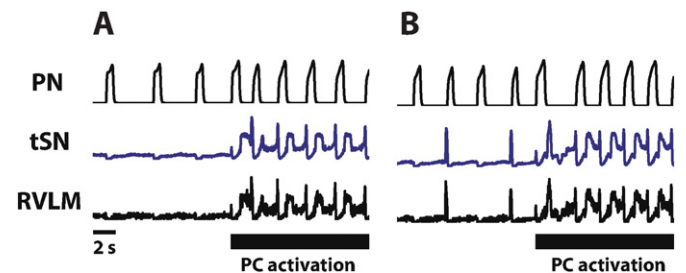


Fig. 8. Simulations of (A) the control model and (B) the CIH model depicting activity in PN and tSN. The amplitude of tSN activity is increased in the CIH model compared to the control model with late-E bursting present.

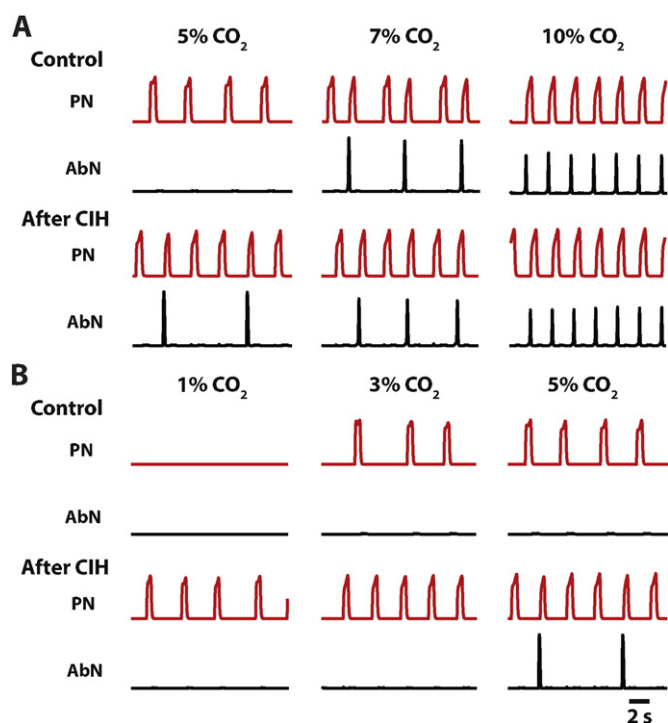


Fig. 9. Simulations of progressive (A) hypercapnia and (B) hypocapnia in PN and AbN in the control model and the CIH model. (A) Simulations reproduce hypocapnic shift in threshold for the emergence of late-expiratory activity in the AbN in the CIH model. (B) Simulations reproduce hypocapnic shift in the onset of respiratory activity of the PN in the CIH model.

(Fig. 6B), and hence, no late-E activity appeared in the AbN and tSN motor outputs (Fig. 5B). Decrease in drive to the RTN also reduces drive distributed to the CPG; RTN suppression induces a reduction in the baseline frequency of the respiratory rhythm.

3.2.4. Simulation of transient activation of peripheral chemoreceptors in CIH rats

The main difference in the effect of peripheral chemoreceptors in CIH compared to naïve rats was a substantial increase in sympatho-excitation (Braga et al., 2006) (Fig. 3). The tonic component of sympatho-excitation in our model was mediated by direct projections from 2nd-order NTS chemoreceptive neurons to the pre-sympathetic RVLM. Activation of this chemosensory drive led to a tonic component to the sympathetic outflow during peripheral chemoreceptor activation by means of this direct projection to RVLM (Fig. 8A). To accommodate an increase in sympatho-excitation in CIH compared to the control model, we increased the amplitude of the peripheral chemoreceptor input by a factor of approximately 2. During peripheral chemoreceptor activation, the firing frequency of 2nd-order NTS chemoreceptive neurons was greater in the CIH model than in the control model. As such, the efficacy of the excitatory projection to RVLM was greater, which causes greater sympathetic outflow in the CIH model upon activation of the peripheral chemoreceptors (Fig. 8B). These effects of increased chemosensory drive in the CIH model were only visible during activation of the peripheral chemoreceptors.

3.2.5. Simulation of progressive hypercapnia and hypocapnia in the naïve model and the CIH model

A hallmark of CIH in the respiratory circuits is a hypocapnic shift in the threshold for the emergence of self-sustained rhythmic respiratory activity (apneic threshold) and a hypocapnic shift in the threshold for the emergence of active expiration. Previously, we described these changes in terms of direct sensitization of the RTN to the partial pressure of CO₂ in the blood (Molkov et al., 2011; Rybak et al., 2012;

Molkov et al., 2014b). The previous model did not describe the mechanism by which CIH induces plasticity in the respiratory CPG. As described above, the pre-I/I population in the pre-BötC of SHR has smaller leak conductance compared to Wistar rats (Moraes et al., 2014). Here, we extend the model to incorporate similar change in the pre-I/I population to explain CIH induced plasticity to the respiratory CPG. Increased excitability of pre-I/I population readily explained a lower apneic threshold after CIH. By adding a glutamatergic excitatory projection from this pre-I/I population to the late-E population in the pFRG, the increased excitability in the pre-BötC was integrated by the pFRG to lower its threshold for activation. This projection mediated a change in the active expiration threshold induced by plasticity to the pre-I/I population in the CIH model.

In the model, we incrementally increased central chemosensory drive in the control and CIH models to simulate progressive increase in blood CO₂ from normocapnia at 5% to mild and then strong hypercapnia at respectively 7% and 10% partial pressure of CO₂ (Fig. 9A). To accommodate progressive hypercapnia in the model, we changed the weight of the CO₂ sensitive drive to RTN-cpg and RTN-late-E at the rate of 0.05 nS per 1% CO₂, which resulted in ~1.2 nS for 7% CO₂ and to ~1.35 nS for 10% CO₂. This simulation was consistent with experiments performed in the arterially perfused preparation where the partial pressure of CO₂ in the perfusate was implemented over the same incremental range (Molkov et al., 2011) (Fig. 1). In the control model, active expiration (marked by the presence of late-E activity in the AbN) emerged at 7% CO₂ (Fig. 9A). The frequency of these late-E AbN bursts increased in a quantal fashion (Molkov et al., 2010; Rubin et al., 2011) from 1:2 AbN bursts per inspiratory PN bursts at 7% CO₂ to 1:1 AbN bursts per inspiratory PN bursts at 10% CO₂. In the CIH model, the threshold for emergence of late-E AbN activity was decreased (Fig. 9A) as in normocapnia (5% partial pressure of CO₂), AbN bursts were already present after CIH conditioning.

We incrementally decreased central chemosensory drive in the control and CIH models to simulate a progressive decrease in blood CO₂ partial pressure from normocapnia at 5% blood CO₂ to mild and then strong hypocapnia - 3% and 1% partial pressure of CO₂ respectively. We accomplished progressive hypocapnia in the model by decreasing the weight of the CO₂ sensitive drive to RTN-cpg and RTN-late-E to 0.72 nS for 3% CO₂ and to 0 nS for 1% CO₂. In the control model, respiratory activity—represented as inspiratory bursts reflected in the PN—persisted in mild hypocapnia (Fig. 9B, Control, 3% CO₂) but disappeared in strong hypocapnia (Fig. 9B, Control, 1% CO₂). After CIH a decrease from 5% to 3% CO₂ eliminated late-E discharges in AbN (Fig. 9B, After CIH). A further decrease to 1% CO₂ did not stop the respiratory rhythm as opposed to the control case. This scenario is similar to findings in the rat (Fig. 1), (Molkov et al., 2011).

4. Discussion

The model presented qualitatively reproduced the effects of peripheral chemoreflex activation in the arterially perfused preparation of decerebrate rats. By changing a subset of biophysical parameters, the model was also able to reproduce the response to progressive hypercapnia and hypocapnia as well as increased sympathoexcitation in CIH. This model provided possible mechanistic explanations to the peripheral chemoreflex response and to plasticity induced by CIH. The model was based on several hypotheses that can be tested in experimental animals (each developed further below): (Hypothesis 1) 2nd-order peripheral chemoreceptive neurons in the NTS project directly to the RTN central chemoreceptors (the anatomical projections were previously confirmed by Takakura et al. (2006)); (Hypothesis 2) sympathetic neurons in the RVLM receive convergent excitatory inputs from late-E (pFRG), a post-I population in the cVRG, and 2nd-order chemoreceptive neurons in the NTS; and (Hypothesis 3) CIH-induced plasticity in the brainstem circuits can be explained by a down-regulation of ohmic leak channels in the pre-I/I population (pre-BötC).

4.1. Peripheral chemoreflex in control rats

During peripheral chemoreceptor stimulation the respiratory frequency substantially increases (Fig. 2) whereas RTN central chemoreceptor activation during hypercapnia does not lead to significant frequency variations (Molkov et al., 2010; Molkov et al., 2014a). Based on this we assumed that NTS peripheral chemoreceptors accelerate phrenic discharges by exciting the inspiratory neurons in the pre-BötC which was reflected in the model by direct excitatory projections from NTS to the pre-I/I population (Fig. 4). This possibility is supported by previous studies showing that microinjections of glutamate in the pre-BötC increase PN frequency *in vivo* and *in situ* while the antagonism of ionotropic glutamatergic receptors in this area eliminated the PN, but not the AbN and tSN responses to peripheral chemoreflex activation *in situ* (Moraes et al., 2011; Moraes et al., 2012c).

Peripheral chemoreceptor activation led to the emergence of late-E discharges in the abdominal and sympathetic nerve activities (Fig. 2). These late-E bursts strongly resembled the discharges appearing in the same nerves during hypercapnia (Molkov et al., 2011). Appearance of late-E activity during hypercapnia is mediated by the increased tonic drive provided by the RTN chemoreceptors (Molkov et al., 2010). Further, late-E discharges emerging in AbN and tSN during peripheral chemoreceptor stimulation can be abolished by pharmacological suppression of the RTN (Moraes et al., 2012a). These facts are consistent with the hypothesis that NTS second order peripheral chemoreceptive neurons send excitatory inputs to the RTN central chemoreceptors (Takakura et al., 2006) (Hypothesis 1). This was implemented in the model as direct excitatory projections from 2nd-order peripheral chemoreceptive NTS neurons to RTN chemoreceptors (Fig. 4).

Activation of peripheral chemoreceptors was accompanied by powerful discharges in HN, cVN, AbN, and tSN motor outputs during the post-inspiratory phase of the respiratory cycle (Fig. 2). This means that activation of 2nd order NTS chemoreceptive cells may have a direct excitatory effect on expiratory neurons. Direct excitation of post-I or aug-E neurons in the BötC compartment of the respiratory CPG would be inconsistent with an increase in the respiratory frequency. Accordingly, we propose that this post-I activity is recruited at the level of pattern formation rather than pattern generation. Previous studies suggested that the pattern formation level in the respiratory CPG is primarily represented by rVRG and cVRG, predominantly containing inspiratory and expiratory neurons, respectively (Rybak et al., 2007; Smith et al., 2007). Accordingly, in the model, we placed a new post-I population in the cVRG.

There is well-documented evidence of direct excitatory projections from 2nd order NTS peripheral chemoreceptive neurons to the RVLM (see Accorsi-Mendonca and Machado (2013) for review) which mediate sympathoexcitatory effect of peripheral chemoreceptor stimulation. Our model implies that there are at least two more indirect pathways mediated by the respiratory neurons (Hypothesis 2).

The first is a consequence of excitatory projections from RTN late-E population to RVLM suggested in our previous publications (Baekey et al., 2010; Molkov et al., 2011; Rybak et al., 2012; Molkov et al., 2014b) to explain appearance of late-E discharges in the sympathetic activity during hypercapnia. The RTN late-E population receives excitatory drive from the RTN central chemoreceptors which increases with blood CO₂ level due to their intrinsic CO₂ chemosensitivity. Our model suggests that an excitatory input from the NTS peripheral chemoreceptors to RTN central chemoreceptors (Takakura et al., 2006), is functionally important to activate RTN late-E neurons and to consequently evoke late-E discharges in the sympathetic nerve during peripheral chemoreceptor stimulation. The critical role of the RTN in the generation of late-E bursts during peripheral chemoreflex was previously demonstrated (Moraes et al., 2012a).

The second indirect pathway is mediated by the post-I population, which we introduced to explain the occurrence of strong post-inspiratory discharges in multiple respiratory and sympathetic motor outputs,

and putatively placed to the cVRG compartment of the respiratory network. This novel population receives inhibition during inspiratory and E2 phases, and can only activate during post-inspiration by an excitatory peripheral chemoreceptor drive from NTS. Apparently, this post-I mediated pathway seems to play a dominant role, since the depression of post-I activity elicited either by the glutamatergic antagonism in the NTS (Costa-Silva et al., 2010) or pontine-medullary transection (Baekey et al., 2008) significantly attenuated the sympatho-excitatory response to peripheral chemoreflex stimulation.

4.2. CIH-induced central and peripheral plasticity

Given that the pre-I/I population of the pre-BötC is a primary target for tonic excitatory drives to the respiratory CPG and that these drives are strongly activated during the peripheral chemoreflex response (Moraes et al., 2014), we speculated that repetitive activation of the peripheral chemoreflex may induce plasticity of channel expression due to prolonged excessive excitation. Recent evidence in SHR indicates a decrease in the leak conductance of pre-inspiratory neurons in the pre-Bötzinger complex (Moraes et al., 2014) which elevates their excitability. Our model shows that similar changes as a result of CIH exposure may explain abovementioned downshifts in the CO₂ thresholds (Hypothesis 3). However, the mechanisms responsible for such plasticity remain to be found.

One possibility is that this change is mediated by downregulation of potassium leak channels. Persistent and repetitive activation of group I metabotropic glutamate receptors over the course of CIH conditioning would increase the catalyzation of diacylglycerol, leading to activation of protein kinase C and the subsequent decrease of the leak conductance through channel protein trafficking (Gabriel et al., 2012). Another example of similar changes consistent with the timescale considered in our study is an excitotoxicity-mediated transcriptional decrease in HCN channel function found to increase excitability of CA1 cells (Adams et al., 2009). In that study an induced increase in synchronous burst duration correlated with a reduction in HCN2 mRNA levels which persisted for at least 7 days. HCN channels are primarily permeable to K⁺ ions, and, hence, their downregulation positively affects the excitability. This is consistent with the recent idea of peripheral chemoreceptor mediated channelopathy within the respiratory network in SHRs (Moraes et al., 2015).

As already mentioned, after CIH conditioning the respiratory CPG exhibits higher respiratory rate and lower CO₂ thresholds for both late-E activity emergence and hypocapnic apnea (Figs. 1, 9). Previously this was explained by increased CO₂ sensitivity of the RTN central chemoreceptors following CIH exposure (Molkov et al., 2011) but no experimental evidence of any intrinsic changes in the central chemoreceptors was available. Our present model provides a different explanation based on increased excitability of the pre-BötC pre-I/I population discussed above. Since this population is a main driver of the inspiratory activity in the network, its increased excitability alone would lead to a lesser dependence on excitatory drive from RTN central chemoreceptors and, hence, to a lower apneic threshold. To explain the lower threshold for late-E emergence, we hypothesize and implement in the model that pre-I/I neurons send excitatory projections to the RTN late-E population (Fig. 4). Due to increased excitability after CIH exposure, pre-I/I neurons increase their firing including the pre-I (late-E) phase and thus provide additional excitation to the RTN late-E population which underlies the emergence of late-E activity at lower CO₂ levels (Fig. 9).

CIH conditioned rats exhibit a stronger peripheral chemoreflex evoked sympathetic response than control animals (Fig. 3). We speculated that this effect reflects stronger activation of the direct sympathoexcitatory pathway rather than indirect inputs from respiratory populations. This assumption is in accord with the fact that CIH exposure increases the duration but not the magnitude of the respiratory response to peripheral chemoreceptor stimulation (Fig. 3). We suggest that the underlying mechanism consists in chronic sensitization of

peripheral chemoreceptors during CIH conditioning which finds strong experimental support (Pawar et al., 2008; Tan et al., 2010; Zoccal et al., 2011; Abdala et al., 2012; Costa-Silva et al., 2012; Kumar and Prabhakar, 2012). That is not to say that baseline facilitation of motoneuron activity in CIH rats is dependent upon peripheral chemoreceptor sensitization. For example, AbN and tSN late-E activity persists despite carotid body transection after CIH conditioning (Zoccal et al., 2008).

Alternative brainstem plasticity could contribute to increased peripheral chemoreflex sympathoexcitation after CIH conditioning. For example glutamatergic transmission in the NTS is augmented in CIH (Costa-Silva et al., 2012). In this case, plasticity of NTS chemoreceptive neural response to peripheral chemoreflex stimulation could amplify the motoneuron responses independent of the strength of the input from the carotid body. Besides, CIH conditioning increases the strength of the purinergic sympathoexcitatory response in the RVLM (Zoccal et al., 2011). This mechanism could account for increased sympathoexcitatory response to peripheral chemoreflex stimulation. In the model we implement that as a greater activity of the 2nd-order chemoreceptive NTS neurons in CIH-conditioned animals as compared to the naïve ones. Our simulations support the plausibility of this assumption (Fig. 8).

5. Summary and conclusions

The generation of late-expiratory bursts in sympathetic activity coupled with the emergence of active expiration has been highlighted as an important mechanism underpinning high levels of sympathetic activity and arterial pressure in rats submitted to CIH (Zoccal et al., 2008; Zoccal et al., 2009; Moraes et al., 2013). Although carotid body chemoreceptors were found to be critical for the development of CIH-induced arterial hypertension (Fletcher et al., 1992), inputs from peripheral chemoreceptors are not required for the maintenance of expiratory component of the sympathetic activity (at least on the time scales studied) since the carotid body removal after CIH exposure did not eliminate late-E activity in the sympathetic nerve (Molkov et al., 2011). In fact, hypocapnia-induced reduction of respiratory drive canceled the sympathetic and abdominal late-E bursts in CIH rats and rescued the normal sympathetic burst pattern (Molkov et al., 2011), indicating that coupling between respiratory and sympathetic networks is a critical mechanisms for maintenance of sympathetic overactivity after CIH exposure. In our study, we sought to identify the potential neural mechanisms required for the development of active expiration and sympathetic overactivity in CIH rats.

In order to simulate neuronal activity of rats conditioned by CIH, a subset of parameters in the CIH model were altered from the values in the control model. These changes reflected central and peripheral plasticity. We modeled central plasticity in the brainstem by increasing the neuronal excitability in the pre-I/I population. The conductance of the leak current in neurons of the pre-I/I population was changed from 2.9 nS to 2.3 nS. This change mediated the hypocapnic shift in apneic threshold and the threshold for the emergence of active expiration (Fig. 9). We mimicked peripheral plasticity due to CIH by increasing the excitatory drive to 2nd-order chemoreceptive neurons in the NTS during peripheral chemoreflex. In the control model, the weight of this drive was 0.75 nS, and it increased in magnitude to 1.6 nS in the CIH model. The effect of this change is only visible during stimulation of the peripheral chemoreflex (Fig. 8).

Our hypothesis implies that the discussed plastic changes in the respiratory network critically depend on the peripheral chemoreceptor input and not on hypoxia per se. This is indirectly supported by multiple experimental studies (see (Paton et al., 2013a) for review) and emphasizes the importance of carotid bodies as a possible therapeutic target for treating neurogenic hypertension (McBryde et al., 2013; Paton et al., 2013b).

Acknowledgements

This study was supported by NIH grant R01 AT008632 to YIM, APL and DZ. IAR is funded by NIH grant R01 NS069220. DZ is funded by São Paulo State Foundation (FAPESP, grant 2013/17251-6). JFRP is funded by the British Heart Foundation. APL is funded by the International Rett Syndrome Foundation. This work utilized the computational resources of the NIH HPC Biowulf cluster. (<http://hpc.nih.gov>).

References

- Abdala, A.P., McBryde, F.D., Marina, N., Hendy, E.B., Engelman, Z.J., Fudim, M., Sobotka, P.A., Gourine, A.V., Paton, J.F., 2012. Hypertension is critically dependent on the carotid body input in the spontaneously hypertensive rat. *J Physiol* 590, 4269–4277.
- Abdala, A.P., Rybak, I.A., Smith, J.C., Paton, J.F., 2009. Abdominal expiratory activity in the rat brainstem-spinal cord in situ: patterns, origins and implications for respiratory rhythm generation. *J Physiol* 587, 3539–3559.
- Accorsi-Mendonça, D., Machado, B.H., 2013. Synaptic transmission of baro- and chemoreceptors afferents in the NTS second order neurons. *Auton. Neurosci.* 175, 3–8.
- Adams, B.E., Reid, C.A., Myers, D., Ng, C., Powell, K., Phillips, A.M., Zheng, T., O'Brien, T.J., Williams, D.A., 2009. Excitotoxic-mediated transcriptional decreases in HCN2 channel function increase network excitability in CA1. *Exp Neurol* 219, 249–257.
- Aicher, S.A., Saravay, R.H., Cravo, S., Jeske, I., Morrison, S.F., Reis, D.J., Milner, T.A., 1996. Monosynaptic projections from the nucleus tractus solitarius to C1 adrenergic neurons in the rostral ventrolateral medulla: comparison with input from the caudal ventrolateral medulla. *J Comp Neurol* 373, 62–75.
- Baekey, D.M., Dick, T.E., Paton, J.F., 2008. Pontomedullary transection attenuates central respiratory modulation of sympathetic discharge, heart rate and the baroreceptor reflex in the in situ rat preparation. *Exp Physiol* 93, 803–816.
- Baekey, D.M., Molkov, Y.I., Paton, J.F., Rybak, I.A., Dick, T.E., 2010. Effect of baroreceptor stimulation on the respiratory pattern: insights into respiratory-sympathetic interactions. *Respir Physiol Neurobiol* 174, 135–145.
- Braga, V.A., Soriano, R.N., Machado, B.H., 2006. Sympathoexcitatory response to peripheral chemoreflex activation is enhanced in juvenile rats exposed to chronic intermittent hypoxia. *Exp Physiol* 91, 1025–1031.
- Briant, L.J., O'Callaghan, E.L., Champneys, A.R., Paton, J.F., 2015. Respiratory modulated sympathetic activity: a putative mechanism for developing vascular resistance? *J Physiol* 593, 5341–5360.
- Caples, S.M., Gami, A.S., Somers, V.K., 2005. Obstructive sleep apnea. *Ann Intern Med* 142, 187–197.
- Carey, R.M., 2013. Resistant hypertension. *Hypertension* 61, 746–750.
- Costa-Silva, J.H., Zoccal, D.B., Machado, B.H., 2010. Glutamatergic antagonism in the NTS decreases post-inspiratory drive and changes phrenic and sympathetic coupling during chemoreflex activation. *J Neurophysiol* 103, 2095–2106.
- Costa-Silva, J.H., Zoccal, D.B., Machado, B.H., 2012. Chronic intermittent hypoxia alters glutamatergic control of sympathetic and respiratory activities in the commissural NTS of rats. *Am. J. Phys. Regul. Integr. Comp. Phys.* 302, R785–R793.
- Dick, T.E., Hsieh, Y.H., Morrison, S., Coles, S.K., Prabhakar, N., 2004. Entrainment pattern between sympathetic and phrenic nerve activities in the Sprague-Dawley rat: hypoxia-evoked sympathetic activity during expiration. *Am. J. Phys. Regul. Integr. Comp. Phys.* 286, R1121–R1128.
- Dudenbostel, T., Calhoun, D.A., 2011. Resistant hypertension, obstructive sleep apnoea and aldosterone. *J. of Hum. Hypertens.*
- Esler, M., 2009. The 2009 Carl Ludwig lecture: pathophysiology of the human sympathetic nervous system in cardiovascular diseases: the transition from mechanisms to medical management. *J Appl Physiol* 108, 227–237.
- Fisher, J.P., Paton, J.F., 2012. The sympathetic nervous system and blood pressure in humans: implications for hypertension. *J Hum Hypertens* 26, 463–475.
- Fletcher, E.C., 2001. Invited review: Physiological consequences of intermittent hypoxia: systemic blood pressure. *J Appl Physiol* 90, 1600–1605.
- Fletcher, E.C., Lesske, J., Culman, J., Miller, C.C., Unger, T., 1992. Sympathetic denervation blocks blood pressure elevation in episodic hypoxia. *Hypertension* 20, 612–619.
- Gabriel, L., Lvov, A., Orthodoxou, D., Rittenhouse, A.R., Kobertz, W.R., Melikian, H.E., 2012. The acid-sensitive, anesthetic-activated potassium leak channel, KCNK3, is regulated by 14-3-3beta-dependent, protein kinase C (PKC)-mediated endocytic trafficking. *J Biol Chem* 287, 32354–32366.
- Go, A.S., Mozaffarian, D., Roger, V.L., Benjamin, E.J., Berry, J.D., Blaha, M.J., Dai, S., Ford, E.S., Fox, C.S., Franco, S., Fullerton, H.J., Gillespie, C., Hailpern, S.M., Heit, J.A., Howard, V.J., Huffman, M.D., Judd, S.E., Kissela, B.M., Kittner, S.J., Lackland, D.T., Lichtman, J.H., Lisabeth, L.D., Mackey, R.H., Magid, D.J., Marcus, G.M., Marelli, A., Matchar, D.B., McGuire, D.K., Mohler ER, 3rd, Moy, C.S., Mussolino, M.E., Neumar, R.W., Nichol, G., Pandey, D.K., Paynter, N.P., Reeves, M.J., Sorlie, P.D., Stein, J., Towfighi, A., Turan, T.N., Virani, S.S., Wong, N.D., Woo, D., Turner, M.B., American Heart Association Statistics C, Stroke Statistics S, 2014. Executive summary: heart disease and stroke statistics—2014 update: a report from the American Heart Association. *Circulation* 129, 399–410.
- Janczewski, W.A., Feldman, J.L., 2006. Distinct rhythm generators for inspiration and expiration in the juvenile rat. *J. Physiol. Lond.* 570, 407–420.
- Kearney, P.M., Whelton, M., Reynolds, K., Muntner, P., Whelton, P.K., He, J., 2005. Global burden of hypertension: analysis of worldwide data. *Lancet* 365, 217–223.
- Konecny, T., Somers, V.K., 2011. Vascular dysfunction in sleep apnea: not just a peripheral concern. *Hypertension* 58, 352–353.

- Koshiya, N., Guyenet, P.G., 1996. Tonic sympathetic chemoreflex after blockade of respiratory rhythmogenesis in the rat. *J Physiol* 491 (Pt 3), 859–869.
- Kumar, P., Prabhakar, N.R., 2012. Peripheral chemoreceptors: function and plasticity of the carotid body. *Comp. Physiol.* 2, 141–219.
- Malpas, S.C., 2010. Sympathetic nervous system overactivity and its role in the development of cardiovascular disease. *Physiol Rev* 90, 513–557.
- McBryde, F.D., Abdala, A.P., Hendy, E.B., Pijacka, W., Marvar, P., Moraes, D.J., Sobotka, P.A., Paton, J.F., 2013. The carotid body as a putative therapeutic target for the treatment of neurogenic hypertension. *Nature communications* 4, 2395.
- Molkov, Y.I., Abdala, A.P., Bacak, B.J., Smith, J.C., Paton, J.F., Rybak, I.A., 2010. Late-expiratory activity: emergence and interactions with the respiratory CpG. *J Neurophysiol* 104, 2713–2729.
- Molkov, Y.I., Shevtsova, N.A., Park, C., Ben-Tal, A., Smith, J.C., Rubin, J.E., Rybak, I.A., 2014a. A closed-loop model of the respiratory system: focus on hypercapnia and active expiration. *PLoS one* 9, e109894.
- Molkov, Y.I., Zoccal, D.B., Baekey, D.M., Abdala, A.P., Machado, B.H., Dick, T.E., Paton, J.F., Rybak, I.A., 2014b. Physiological and pathophysiological interactions between the respiratory central pattern generator and the sympathetic nervous system. *Prog Brain Res* 212, 1–23.
- Molkov, Y.I., Zoccal, D.B., Moraes, D.J., Paton, J.F., Machado, B.H., Rybak, I.A., 2011. Intermittent hypoxia-induced sensitization of central chemoreceptors contributes to sympathetic nerve activity during late expiration in rats. *J Neurophysiol* 105, 3080–3091.
- Moraes, D.J., Bonagamba, L.G., Zoccal, D.B., Machado, B.H., 2011. Modulation of respiratory responses to chemoreflex activation by L-glutamate and ATP in the rostral ventrolateral medulla of awake rats. *Am. J. Phys. Regul. Integr. Comp. Phys.* 300, R1476–R1486.
- Moraes, D.J., da Silva, M.P., Bonagamba, L.G., Mecawi, A.S., Zoccal, D.B., Antunes-Rodrigues, J., Varanda, W.A., Machado, B.H., 2013. Electrophysiological properties of rostral ventrolateral medulla presympathetic neurons modulated by the respiratory network in rats. *J Neurosci* 33, 19223–19237.
- Moraes, D.J., Dias, M.B., Cavalcanti-Kwiatkoski, R., Machado, B.H., Zoccal, D.B., 2012a. Contribution of the retrotrapezoid nucleus/parafacial respiratory region to the expiratory-sympathetic coupling in response to peripheral chemoreflex in rats. *J Neurophysiol* 108, 882–890.
- Moraes, D.J., Machado, B.H., Paton, J.F., 2014. Specific respiratory neuron types have increased excitability that drive presympathetic neurones in neurogenic hypertension. *Hypertension* 63, 1309–1318.
- Moraes, D.J., Machado, B.H., Paton, J.F., 2015. Carotid body overactivity induces respiratory neurone channelopathy contributing to neurogenic hypertension. *J Physiol* 593, 3055–3063.
- Moraes, D.J., Zoccal, D.B., Machado, B.H., 2012b. Medullary respiratory network drives sympathetic overactivity and hypertension in rats submitted to chronic intermittent hypoxia. *Hypertension* 60, 1374–1380.
- Moraes, D.J., Zoccal, D.B., Machado, B.H., 2012c. Sympathoexcitation during chemoreflex active expiration is mediated by L-glutamate in the RVLM/Botzinger complex of rats. *J Neurophysiol* 108, 610–623.
- Narkiewicz, K., van de Borne, P.J., Montano, N., Dyken, M.E., Phillips, B.G., Somers, V.K., 1998. Contribution of tonic chemoreflex activation to sympathetic activity and blood pressure in patients with obstructive sleep apnea. *Circulation* 97, 943–945.
- Paton, J.F., 1996. A working heart-brainstem preparation of the mouse. *J. Neurosci. Methods* 65, 63–68.
- Paton, J.F., Ratcliffe, L., Hering, D., Wolf, J., Sobotka, P.A., Narkiewicz, K., 2013a. Revelations about carotid body function through its pathological role in resistant hypertension. *Curr. Hypertens. Rep.* 15, 273–280.
- Paton, J.F., Sobotka, P.A., Fudim, M., Engleman, Z.J., Hart, E.C., McBryde, F.D., Abdala, A.P., Marina, N., Gourine, A.V., Lobo, M., Patel, N., Burchell, A., Ratcliffe, L., Nightingale, A., 2013b. The carotid body as a therapeutic target for the treatment of sympathetically mediated diseases. *Hypertension* 61, 5–13.
- Pawar, A., Peng, Y.J., Jacono, F.J., Prabhakar, N.R., 2008. Comparative analysis of neonatal and adult rat carotid body responses to chronic intermittent hypoxia. *J. Appl. Physiol.* (1985) 104, 1287–1294.
- Pedrosa, R.P., Drager, L.F., Gonzaga, C.C., Sousa, M.G., de Paula, L.K., Amaro, A.C., Amodeo, C., Bortolotto, L.A., Krieger, E.M., Bradley, T.D., Lorenzi-Filho, G., 2011. Obstructive sleep apnea: the most common secondary cause of hypertension associated with resistant hypertension. *Hypertension* 58, 811–817.
- Rubin, J.E., Bacak, B.J., Molkov, Y.I., Shevtsova, N.A., Smith, J.C., Rybak, I.A., 2011. Interacting oscillations in neural control of breathing: modeling and qualitative analysis. *J. Comput. Neurosci.* 30, 607–632.
- Rybak, I.A., Abdala, A.P., Markin, S.N., Paton, J.F., Smith, J.C., 2007. Spatial organization and state-dependent mechanisms for respiratory rhythm and pattern generation. *Prog. Brain Res.* 165, 201–220.
- Rybak, I.A., Molkov, Y.I., Paton, J.F.R., Abdala, A.P.L., Zoccal, D.B., 2012. Modeling the autonomic nervous system. *Primer on the Autonomic Nervous System* (Robertson, D. et al., eds). Elsevier Inc.
- Simms, A.E., Paton, J.F., Pickering, A.E., Allen, A.M., 2009. Amplified respiratory-sympathetic coupling in the spontaneously hypertensive rat: does it contribute to hypertension? *J. Physiol.* 587, 597–610.
- Smith, J.C., Abdala, A.P., Koizumi, H., Rybak, I.A., Paton, J.F., 2007. Spatial and functional architecture of the mammalian brain stem respiratory network: a hierarchy of three oscillatory mechanisms. *J. Neurophysiol.* 98, 3370–3387.
- Takakura, A.C., Moreira, T.S., Colombari, E., West, G.H., Stornetta, R.L., Guyenet, P.G., 2006. Peripheral chemoreceptor inputs to retrotrapezoid nucleus (RTN) CO₂-sensitive neurons in rats. *J. Physiol.* 572, 503–523.
- Tan, Z.Y., Lu, Y., Whiteis, C.A., Simms, A.E., Paton, J.F., Chappelle, M.W., Abboud, F.M., 2010. Chemoreceptor hypersensitivity, sympathetic excitation, and overexpression of ASIC and TASK channels before the onset of hypertension in SHR. *Circ. Res.* 106, 536–545.
- Williams, S.K., Ravenell, J., Jean-Louis, G., Zizi, F., Underberg, J.A., McFarlane, S.I., Ogedegbe, G., 2010. Resistant hypertension and sleep apnea: pathophysiologic Insights and Strategic Management. *Curr. Diab. Rep.*
- Zoccal, D.B., 2015. Peripheral chemoreceptors and cardiorespiratory coupling: a link to sympatho-excitation. *Exp. Physiol.* 100, 143–148.
- Zoccal, D.B., Bonagamba, L.G., Paton, J.F., Machado, B.H., 2009. Sympathetic-mediated hypertension of awake juvenile rats submitted to chronic intermittent hypoxia is not linked to baroreflex dysfunction. *Exp. Physiol.* 94, 972–983.
- Zoccal, D.B., Bonagamba, L.G.H., Oliveira, F.R.T., Antunes-Rodrigues, J., Machado, B.H., 2007. Increased sympathetic activity in rats submitted to chronic intermittent hypoxia. *Exp. Physiol.* 92, 79–85.
- Zoccal, D.B., Huidobro-Toro, J.P., Machado, B.H., 2011. Chronic intermittent hypoxia augments sympatho-excitatory response to ATP but not to L-glutamate in the RVLM of rats. *Auton. Neurosci.* 165, 156–162.
- Zoccal, D.B., Simms, A.E., Bonagamba, L.G., Braga, V.A., Pickering, A.E., Paton, J.F., Machado, B.H., 2008. Increased sympathetic outflow in juvenile rats submitted to chronic intermittent hypoxia correlates with enhanced expiratory activity. *J. Physiol.* 586, 3253–3265.